Glial activation in APP/PS1 mice is associated with infiltration of IFNγ-producing cells

Ronan J. Kelly*, Aedín M. Minogue*†, Anthony Lyons, Raasay S. Jones, Tara C. Browne, Derek A. Costello, Stephanie Denieffe, Catherine O'Sullivan, Thomas J. Connor, and Marina A. Lynch

Trinity College Institute of Neuroscience,

Trinity College,

Dublin 2,

Ireland.

*These authors contributed equally to this work.

†Correspondance: Email: aminogu@tcd.ie; Tel: 353-1-896-8476; Fax: 353-1-896-3545.

Email addresses : rjkelly@tcd.ie; alyons@smu.ky; jonesrs@tcd.ie; brownetc@tcd.ie; decostel@tcd.ie; deniefs@tcd.ie; osullc12@tcd.ie; connort@tcd.ie; lynchma@tcd.ie

Running title: Infiltrating immune cells in APP/PS1 mice

ABSTRACT

Whereas the classical histological hallmarks of Alzheimer's disease (AD) are deposition of amyloid-containing plaques and development of neurofibrillary tangles, there is also clear evidence of inflammatory changes accompanied by the presence of activated microglia and astrocytosis. However, at this time it remains uncertain whether inflammatory changes contribute to pathogenesis of the disease or if they are secondary to deposition of amyloid-β or other pathological changes. A greater understanding of the sequence of events would clearly improve development of strategies to delay progression of the disease. There is a realistic expectation that advances in imaging technology may provide the key to uncovering this sequence. In this study, we employed non-invasive imaging techniques to examine changes in tissue state in hippocampus and cortex of transgenic mice which overexpress amyloid precursor protein and presenilin 1 and show that the observed increase in T_1 relaxation time was associated with astrogliosis while the decrease in T_2 relaxation time was associated with microglial activation. We explored the possibility that interferon-γ might trigger glial activation and demonstrate a genotype-related infiltration of macrophages and natural killer cells, which release interferon-γ. The evidence suggests that IFNγ triggers glial activation and expression of proinflammatory cytokines, and these changes, in turn, contribute to the decrease in long-term potentiation.

Key words: Natural killer (NK) cells, macrophages, glial activation, T_1 and T_2 relaxation times.

INTRODUCTION

The deposition of amyloid-β (Aβ) in the brain is considered by several research teams as a potential trigger for a sequence of events which eventually leads to synaptic and neuronal dysfunction, and the consequent impaired cognitive function which characterizes Alzheimer's disease (AD). In AD and animal models of the disease, Aβ plaques are decorated by activated glia and some groups have interpreted this finding as an indication that Aβ increases activation of both microglia and astrocytes; this is supported by the fact that Aβ induces microglial activation and triggers astrocytosis *in vitro*, an effect mimicked by Aβ injection *in vivo* [1, 2]. However, it has also been proposed that inflammatory changes, consequent upon persistent glial activation, may contribute to the early pathogenic changes [3]. Thus the inflammatory cytokines TNFα and IL-1β, which are released from activated glia, increase γ-secretase activity [4] while expression of amyloid precursor protein (APP) and β-secretase are also increased by inflammatory cytokines [5]. A specific role for IL-1β is suggested by the finding that a blocking antibody reduces Aβ accumulation in a triple transgenic mouse model of AD [6]. These reports suggest that glial activation may contribute to the pathology and are consistent with the idea that 'inflammaging' may constitute a prodromal AD condition [7]. However this view may also imply that the ability of microglia to adopt their deactivated or alternatively activated states may be altered, perhaps due to decreased expression of factors which induce a shift in activation states such as NADPH oxidase [8] or increased signalling through toll-like receptors which prevents microglia adopting an immunoregulatory phenotype [9].

One of the major challenges in neuroscience is to identify a mechanism by which these changes can be non-invasively recognized to permit early intervention and maximize the

chance of impeding progression from prodromal conditions to AD. In this context, magnetic resonance imaging (MRI) has been a key development and combined analysis of changes in different parameters and histological changes in animal models of AD has provided some understanding of the anatomical correlates which underlie specific changes. Relaxometry, which measures the time taken to return to the baseline energy state following removal of the radio frequency pulse, is a powerful tool in the analysis of tissue states; T_1 relaxation time increases in conditions where there is axonal loss [10] or increased tissue water [11], whereas decreased T_2 relaxation time is associated with iron deposition in tissue [12-14]. Changes in both have been linked with activation of glia following acute ischaemic insult with evidence of an increase in T_1 relaxation time correlating with astrocytosis [15] and a decrease in T_2 relaxation correlating with microglial activation [16].

Here we set out to assess whether the predicted activation of astrocytes and microglia in APP/PS1 mice might be accompanied by changes in T_1 and T_2 relaxometry and to assess whether glial activation might be triggered by infiltration of cells which might induce an inflammatory microenvironment.

METHODS

Animals

Groups of 13-14 month-old (weighing 31g-56g) APPswe/PS1dE9 mice and wildtype littermate controls were used in this study. Mice purchased from the Jackson Laboratory (US) were used to form breeding pairs with C57BL/6 mice and were bred in an SPF housing facility in the Bio-resources Unit, Trinity College, Dublin. In one experiment, wildtype mice were anaesthetized with an intraperitoneal injection of Avertin (20µl/g; Sigma Aldrich, Ireland) and injected intracerebroventricularly with IFNγ (5µl; 50ng/ml in PBS) or an equivalent volume of saline and, 4 hours later, were killed by decapitation. Tissue was taken for preparation of cryostat sections (see below) and mRNA analysis. Mice were maintained under veterinary supervision in a controlled environment (12-hour light-dark cycle; 22-23°C) for the duration of the experiment. Animal experimentation was performed under a licence granted by the Minister for Health and Children (Ireland) under the Cruelty to Animals Act 1876 and the European Community Directive, 86/609/EEC, and in accordance with local ethical guidelines.

MRI

MRI analysis was carried out on a small rodent Bruker Biospec (Bruker Biospin, Germany) system with a 7 Tesla magnet and a 30 cm core to evaluate T_1 and T_2 relaxation times. Mice were anaesthetized using isoflurane, placed into an MR-compatible cradle and positioned in a stereotaxic frame. Anaesthesia was maintained by delivery of a mixture of isoflurane and oxygen administered by mechanical ventilator (1.5 – 2 % at 1 litre/minute of

100% oxygen). Respiration rate was monitored and body temperature was controlled throughout.

A rapid acquisition with relaxation enhancement (RARE) with variable repetition time (RARE-VTR) scan was employed to assess T_1 relaxation times; the scan time was 8 minutes, 43 seconds. A single slice scan (128 x 128 voxels), located 2mm posterior to Bregma, enabled relaxometry times to be obtained from cortical and hippocampal tissue. T_1 relaxometry data were acquired by varying the repetition times (TR) using values ranging from 300ms to 8000ms (TR values: 300, 589.116, 942.255, 1396.084, 2031.981, 3103.081, and 8000.000ms) with an echo time (TE) of 25.27ms and RARE factor = 4. T_1 relaxation times were calculated using the ISA (Image Sequence Analysis) software within the Bruker software package. T_1 relaxation times were fitted to a mono-exponential rise function, exported and analysed in the ImageJ software program. All ROIs were drawn with reference to a standardised mouse brain atlas (Paxinos and Franklin, 1995).

A 9 slice, 8 echo multi-slice multi-echo (MSME) scan was used to quantify T_2 relaxometry times in a scan time of 8 minutes, 32 seconds. These images had the same position as that of the T_1 measurements and a shared geometry of 128 x 128 voxels per slice. The scan parameters were as follows: effective TEs: 12.64, 25.27, 37.91, 50.55, 63.19, 75.82, 88.46, 101.1ms; TR: 2000ms. This allowed for co-localisation of data between the two types of relaxometry assessed in this study. The raw data from the T_2 MSME scan were exported to Interactive Data Language (IDL) and analysed using an in-house scripting procedure, producing a voxelwise linear fitting to the logarithm of the data on the entire data set. The middle 5 echo times were used to create a parametric, quantitative T_2 map that was exported to ImageJ. ROIs were drawn with reference to a

standardised mouse brain atlas (Paxinos and Franklin, 1995) and T_2 relaxation times calculated bilaterally for each hemisphere in 2 adjacent slices, and averaged for each mouse.

Analysis of LTP

A separate cohort of 14 month-old wildtype and APP/PS1 mice were used for preparation of hippocampal slices and analysis of LTP as previously described [17]. Briefly, hippocampal slices (400μm) were maintained at room temperature (21-23°C), in oxygenated artificial cerebrospinal fluid (aCSF; composition in mM: 125 NaCl, 1.25 KCl, 2 $CaCl_2$, 1.5 $MgCl_2$, 1.25 KH_2PO_4, 25 $NaHCO_3$, and 10 D-glucose). For electrophysiological recording, slices were transferred to a submerged recording chamber and perfused with oxygenated aCSF containing 2mM $CaCl_2$ (2-3ml/minute; 21-23°C). To facilitate recording in slices from older wildtype and APP/PS1 slices (Figure 6e), the perfusate contained the $GABA_A$ receptor antagonist, SR95531 (6μM; Ascent Scientific, UK), and a surgical incision made between areas CA1 and CA3 to limit the propagation of epileptiform activity. The Schaffer collateral-commissural pathway was stimulated at 0.033Hz (0.1ms duration), field excitatory postsynaptic potentials (EPSPs) were evoked in CA1 stratum radiatum and stable baseline EPSPs were recorded for a minimum of 15-20 minutes prior to application of theta-burst stimulation [TBS; 10 trains (4 pulses at 100 Hz) repeated at 5 Hz]. To assess the effects of IFNγ on LTP (Figure 10G), slices prepared from 5-7 month-old C57BL/6J mice were perfused with aCSF containing either mouse recombinant IFNγ (1μg/ml; R & D Systems, UK) or vehicle control (0.001% BSA; Sigma-Aldrich, UK) for 30 minutes prior to application of TBS, which was maintained for the duration of the experiment. Data were

acquired using WinWCP v4.0.7 software (Dr J Dempster, Strathclyde, UK) and evoked EPSPs were normalised to the mean EPSP slope recorded in the 5 minute period prior to TBS. LTP was measured as the mean % EPSP slope in the final 5 minutes of recording (55-60 minute following induction).

Detection of SDS-soluble and insoluble Aβ

Soluble and insoluble Aβ were extracted from snap-frozen brain tissue. Tissue was homogenized in 5 volumes (w/v) buffer (50mM NaCl, 1% SDS (w/v), pH10) containing phosphatase and protease inhibitor cocktails (Sigma, UK) and centrifuged at 15,000rpm for 40 minutes at 4°C. SDS-soluble Aβ was assessed in supernatant and insoluble Aβ isolated from the pellets using 5M guanidine. Soluble Aβ concentrations were assessed using 96-well multi-spot 4G8 Aβ triple ultra-sensitive assay kits (MesoScale Discovery, USA). Plates were read using a sector Imager plate reader and concentration of Aβ in the samples determined with reference to the standard curve prepared using recombinant $A\beta_{1-38}$, $A\beta_{1-40}$ and $A\beta_{1-42.}$ Concentrations of Aβ in serum were determined and calculated using the same method described above except that Blocker G was omitted from the detection antibody solution.

Analysis of cytokines

IL-1β, TNFα, IL-2, IL-12p70 and IFNγ were assessed using Multi-plex TH1/TH2 plates (MesoScale Discovery, US). Briefly, tissue was homogenized (SDS/NaCl, pH 10), centrifuged at 15,000rpm for 40 minutes at 4°C and the supernatant sample was taken for cytokines analysis. 96 well plates were blocked, washed, and detection antibody added

according to the manufacturer's instructions. Samples, or standards (0-10,000 pg/ml), prepared in 1% Blocker A solution, were added, incubation proceeded for 2 hours at room temperature and plates were washed. Read buffer was added and the plate was read immediately using a Sector Imager plate reader. Cytokine concentrations were evaluated with reference to the standard curves.

Immunohistochemistry

Cryostat sections from APP/PS1 and wildtype mice were prepared for CD11b and GFAP staining as previously described [18]. Sections were incubated initially in the presence of 10% rabbit or goat serum (Vector Laboratories, UK) to block non-specific binding and overnight with rat anti-mouse CD11b primary antibody (1:100 in PBS containing 5% rabbit serum; AbD Serotec, UK) or for 90 minutes at room temperature with rabbit anti-mouse GFAP primary antibody (1:2000 dilution in PBS containing 1% bovine serum albumin (BSA); Dako, UK). In the case of CD11b staining, sections were washed in PBS and incubated in biotinylated rabbit anti-rat secondary antibody (1:200 in PBS containing 5% rabbit serum; Vector Laboratories, UK) for 2 hours at room temperature. In the case of GFAP staining, sections were washed and incubated in biotinylated goat anti-rabbit secondary antibody (1:200 in PBS containing 1% BSA; Vector Laboratories, UK) for 40 minutes at room temperature. Thereafter, sections were washed and incubated for 30 minutes in Vectastain Elite ABC reagent (Vector Laboratories, UK), for 10 minutes in 3 diaminobenzidine (DAB)-enhanced liquid substrate (Sigma-Aldrich, UK) and counterstained with 1% methyl green (Sigma-Aldrich, UK). Sections were rinsed in dH_2O and dehydrated through graded alcohols and immersed in 100% xylene (VWR International

UK). Coverslips were mounted onto the slides using DPX (RA Lamb, UK) and viewed on an Olympus IX51 light microscope with a built-in camera (Olympus, Japan). Images of DAB-enhanced CD11b and GFAP positive staining were analysed using the Immunoratio plugin (http://imtmicroscope.uta.fi/immunoratio/) available for the ImageJ software package [19] using the following settings: image scale for detection of nuclei 9.3 pixels/μm, brown threshold adjustment -50, blue threshold adjustment +15. The mean percentage DAB enhancement/total nuclear area assessed in cortical and hippocampal regions is presented.

PCR analysis of markers of glial activation

RNA was isolated from cortical brain tissue using Nucleospin® RNAII KIT (Macherey-Nagel, Duren, Germany) and cDNA was prepared using High-Capacity cDNA RT kit according to the manufacturer's instructions (Applied Biosystems, UK). Real-time PCR for the detection of *CD11b, MHCII, GFAP, TNFα* and *IL-6* mRNA was performed with predesigned Taqman gene expression assays (Applied Biosystems, UK). The assay IDs were as follows: *CD11b* Mm00434455_ml, *MHCII* Mm00439221_m1, *GFAP* Mm01253033_ml, *TNFα* (Mm00443258_m1) and *IL-6* (Mm00446191_m1). Samples were assayed on an Applied Biosystems 7500 Fast Real-Time PCR machine and gene expression was calculated relative to the endogenous control samples (β-actin) to give a relative quantification (RQ) value (2^{-DDCT}, where CT is threshold cycle).

Flow Cytometry

Whole brain tissue from one hemisphere was harvested in Hank's Balanced Salt Solution (HBSS) containing 3% fetal bovine serum (FBS), dissociated through a cell strainer (70μm) and centrifuged at 170 x *g* for 10 minutes. The pellet was resuspended in PBS containing collagenase D (1mg/ml) and DNAse I (10μg/ml), incubated for 30 minutes at 37°C with gentle agitation and centrifuged at 170 x *g* for 10 minutes. Cells were resuspended in 1.088 g/ml Percoll (9ml), underlaid with 1.122 g/ml Percoll (5ml), overlaid with 1.072 g/ml Percoll (9ml), 1.030 g/ml Percoll (9ml) and PBS (9ml) and centrifuged at 1250 x *g* for 45 minutes. Mononuclear cells, harvested at the 1.088:1.072g/ml and 1.072:1.030g/ml interfaces were removed, washed 3 times with FACS buffer (2% FBS, 0.1% NaN_3 in PBS) and blocked for 15 minutes with mouse Fc block (BD Biosciences, UK). Cells were incubated with allophycocyanin rat anti-mouse CD11b, PE-Cy™7 rat anti-mouse CD45, PE-Cy™5 CD8 and phycoerythrin rat anti-mouse NKp46 (all BD Biosciences, UK) and Alexa Fluor 488 rat anti-mouse CD68 (AbD Serotec, UK), diluted (1:200) in FACS buffer. Immunofluorescence analysis was performed on a DAKO CyAn-ADP 7 colour flow cytometer (DAKO Cytomation, UK) with FlowJo v7.6.5 software. Microglia, macrophages and NK cells were identified as $CD11b^{+}CD45^{low}$, $CD11b^{+}CD45^{hi}$ and $NKp46^{+}CD8^{+}CD11b^{-}$ respectively.

Isolation of primary microglia

Cortices of 1 day-old Wistar rats (Trinity College, Dublin, Ireland) were removed, cross-chopped and incubated for 25 minutes at 37°C in Dulbecco's Modified Eagle's Medium (DMEM, Invitrogen, UK) supplemented with 10% Foetal Bovine Serum (Invitrogen, UK) and 50 U/ml penicillin/streptomycin (Invitrogen, UK). To prepare purified microglia, cells

were grown in T25 flasks in DMEM. After 12 days the flasks were shaken for 2 hours at 110 rpm, at room temperature and tapped several times to remove non-adherent microglia. The supernatants were removed from the flask and centrifuged at 2000 rpm for 3 minutes at 21°C. The pellet was resuspended in DMEM and the cells were counted. Cells were pipetted into 6 well plates at a density of $5x10^4$cells/cm^2. Isolated microglia were treated with IFNγ (50ng/ml) or vehicle for 24 hours after which time supernatant concentrations of TNFα and IL-6 were assessed by ELISA and cell surface expression of CD11b, CD86 and MHC11 was assessed by flow cytometry.

RESULTS

We used MRI to compare T_2 relaxation time in the brains of wildtype and APP/PS1 mice. The colour-enhanced images indicate marked differences in several areas of the brain of APP/PS1 (Figure 1B), compared with wildtype (Figure 1A), mice and quantitative analysis revealed a significant decrease in T_2 relaxation time in cortex and hippocampus of APP/PS1 mice (*$p < 0.05$; ***$p < 0.001$; Student's *t*-test for Independent means; Figure 1C,D). Analysis of data from other areas of the brain indicate that no significant changes were observed in corpus callosum or thalamus, but were generally confined to cortical and hippocampal regions (Table 2). We, and others, have reported that increased microglial activation is associated with decreased T_2 relaxation time [16, 18] and this finding is confirmed here. Thus increased CD11b immunoreactivity was observed in sections

prepared from APP/PS1 (Figure 1F and H), compared with wildtype, (E and G) mice and similar increases were identified in cortex (Figure 1E,F) and hippocampus (Figure 1G,H); there was a significant increase in the ratio of DAB/nuclear area in cortex and hippocampus (**$p < 0.01$; Student's *t*-test for Independent means; Figure 1I,J respectively). Significant increases in CD11b mRNA (K) and in the number of $CD11b^+$ $CD68^+$ cells (L,M) in tissue prepared from APP/PS1 mice (***$p < 0.001$; Student's *t*-test for Independent means) provided further evidence of microglial activation in transgenic mice. It is important to note that T_2 relaxation time decreases in an age-related manner in wildtype mice and that this is accompanied by enhanced CD11b immunoreactivity (Supplementary Figure 1).

Analysis of T_1 relaxation time (as indicated by the colour change from yellow to orange/red) revealed a marked increase throughout the brain of APP/PS1 mice, compared with wildtype mice (Figure 2A,B). Quantitative analysis revealed significant increases in cortex and hippocampus (*$p < 0.05$; **p 0.01; Student's *t*-test for Independent means; Figure 2C,D). Analysis of data from other areas of the brain indicated that significant changes were observed in cortical and hippocampal regions but not in the corpus callosum or thalamus (Table 2). A correlation between astroglial activation and T_1 relaxation time has been reported in animals following acute ischaemic injury [15] and in aged animals [20] and the present data confirm this correlation. Thus GFAP immunoreactivity, which is an indicator of astrocytic activation, was markedly increased in sections prepared from the cortex of APP/PS1 mice (Figure 2F) compared with wildtype mice (Figure 2E). Similarly, marked GFAP immunoreactivity was observed in hippocampus of APP/PS1 mice compared with wildtype mice (Figure 2; compare H with G); there was a significant increase in the ratio of DAB/nuclear area in cortex and hippocampus (***$p < 0.001$;

Student's *t*-test for Independent means; Figure 2I,J respectively). Consistently, GFAP mRNA was also increased in cortex of APP/PS1 mice compared with wildtype mice (***p < 0.001; Student's *t*-test for Independent means; Figure 2K).

Activated microglia and astrocytes produce inflammatory cytokines and the genotype-associated glial activation described here was associated with increased hippocampal concentrations of IL-1β, TNFα, IL-2 and IL-12 (*p < 0.05; **p < 0.01; ***p < 0.001; Student's *t*-test for Independent means; Figure 3A-D). Increased inflammatory cytokine concentrations negatively impact on synaptic plasticity and IL-1β, TNFα and IL-2 have previously been shown to inhibit LTP [20-22]. Here we report that TBS-induced LTP was significantly attenuated in hippocampal slices prepared from APP/PS1 mice compared with wildtype mice (p < 0.0001, Student's *t*-test for Independent means; Figure 3E).

One of the most potent activators of microglial activation is IFNγ, which is released primarily by immune cells and to a very limited extent if at all from resident cells in the CNS. However IFNγ concentration was significantly increased in hippocampus of APP/PS1 mice compared with wildtype mice (**p < 0.01; Student's *t*-test for Independent means; Figure 4A). One possible explanation for this is that there was significant infiltration of NK cells into the CNS in APP/PS1 mice (***p < 0.001; Student's *t*-test for Independent means; Figure 4B). There was also a 4-fold increase in $CD11b^{+}$ $CD45^{+}$ macrophages in tissue prepared from APP/PS1, compared with wildtype, mice (***p < 0.001; Student's *t*-test for Independent means; Figure 4C) and the proportion of these cells which expressed CD68 was also significantly greater in APP/PS1 mice (**p < 0.01; Student's *t*-test for Independent means; Figure 4D).

To assess the possible role of IFNγ in triggering microglial activation, a cohort of wildtype mice were injected intracerebroventricularly with IFNγ (5µl; 50ng/ml in PBS) and assessed 4 hours later for evidence of glial activation. IFNγ increased CD11b and GFAP immunoreactivity in hippocampus (Figure 5A and C respectively) and also increased mRNA expression of the microglial marker, MHCII (**$p < 0.01$; Student's *t*-test for Independent means; Figure 5B) and the astroglial marker, GFAP (*$p < 0.05$; Student's *t*-test for Independent means; Figure 5D). Significant IFNγ-induced increases in mRNA expression of 2 inflammatory cytokines, TNFα and IL-6 were also observed (*$p < 0.05$; Student's *t*-test for Independent means; Figure 5E,F). Importantly, LTP recorded from hippocampal slices in the presence of IFNγ (1µg/ml) was significantly reduced, relative to that recorded under control conditions ($p < 0.01$; Student's *t*-test for Independent means; Figure 5G).

To ensure changes observed in microglial activation occurred due to the presence of IFNγ, primary microglia were prepared and treated with IFNγ (50ng/ml) for 24 hours (Figure 6). Treatment of isolated microglia with IFNγ significantly enhanced the expression of cell surface molecules such as CD86 and MHCII (**$p < 0.01$; Student's *t*-test for Independent means; Figure 6A and B respectively) and the release of proinflammatory cytokines TNFα and IL-6 (***$p < 0.001$; Student's *t*-test for Independent means; Figure 6C and D respectively). These results parallel those observed *in vivo*.

DISCUSSION

Glial activation is a consistently-described feature of AD and animal models of the disease but the trigger responsible for glial activation is unclear. In this study we have identified a potential sequence of events, initiated by infiltration of IFNγ-producing cells, which leads to this change and ultimately exerts a negative impact on LTP. The data describe a relationship between microglial activation and T_2 relaxation time, and astroglial activation and T_1 relaxation time, opening the possibility that development of changes in microglial activation may be tracked non-invasively particularly as age-related decreases in T_2 relaxation times closely paralleled age-related increases in CD11b immunoreactivity.

Aβ accumulation is detectable in the brain of APP/PS1 transgenic mice at an early age [23] and increases with age [24]. Predictably, increased concentrations of soluble and insoluble $A\beta_{1\text{-}40}$ and $A\beta_{1\text{-}42}$ were evident throughout the brain in the 14 month-old APP/PS1 mice used in this study, as reported by others [25, 26]. Accumulation of Aβ in the brain of APP/PS1 mice is accompanied by several changes including microglial activation [12, 27] and CD11b immunoreactivity and CD11b mRNA were markedly enhanced in tissue prepared from APP/PS1 mice used in the present study; an increase in the number of CD11b-positive cells which expressed CD68 was also demonstrated in tissue prepared from APP/PS1 mice. Microglial activation in APP/PS1 mice has been identified by an increased Iba1 immunoreactivity [28], coupled with increased [^{11}C](R)-PK11195 binding as revealed by positron emission tomography PET [29] and the present data show that it was also associated with a decrease in T_2 relaxation time. An inverse correlation between T_2 relaxation and microglial activation has been observed in different models of inflammation, including aged animals [16, 18, 30]. Accumulation of iron, which occurs in activated microglia, at least in

APP/PS1 mice [12], is considered to contribute to the change in T_2 relaxation time [31], although the combination of iron accumulation and Aβ deposition may be particularly important in inducing the change [31, 32]. GFAP immunoreactivity, which is indicative of astrocytic activity, was also increased in APP/PS1 mice which concurs with previous data [33]. Here, the GFAP immunoreactivity was accompanied by an increase in T_1 relaxation time and this is consistent with the previously-reported positive correlation between astrocytic activation and T_1 relaxation time in aged animals [20] and following acute insult [15].

Both Aβ accumulation and glial activation have been associated with deficits in neuronal function; for example, spatial learning is impaired in some transgenic models of AD including APP/PS1 mice [27, 34, 35], and impaired spatial learning also accompanies glial activation, for example in aged animals [20], LPS-treated animals [36] and Aβ-treated animals [37, 38]. LTP is also decreased in each of these conditions [20, 39-41] and some, but not all researchers, report that LTP is decreased in APP/PS1 mice [25, 39, 42, 43]. The present data indicate that LTP induced by theta-burst stimulation was markedly decreased in area CA1 of 14 month-old APP/PS1 mice and this was associated with increased expression of the inflammatory cytokines IL-1β, TNFα and IL-2, all of which exert a negative impact on LTP [20-22]. Increased expression of inflammatory cytokines commonly accompanies glial activation and both have been associated with increased Aβ accumulation and deficits in synaptic plasticity observed in APP/PS1 mice [12, 27]. Indeed modulation of microglial activation by knocking out CD40 [44] or by treating mice with rosiglitazone [27] or polyunsaturated fatty acids [45], which decrease microglial activation [20, 41, 46], improves spatial learning in models of AD. Despite these findings and the

likelihood that inflammation plays a role in the early stages of AD, modulation of glial activation is not therapeutically valuable in established AD although its benefit, if any, in very early prodromal conditions remains to be determined.

One of the most potent activators of microglia is IFNγ [47, 48], but there is little evidence to suggest that it is released from resident cells in the brain. Here we demonstrate that glial activation is associated with infiltration of macrophages and NK cells, both of which release IFNγ in response to IL-12 and IL-2, as well as IL-18 [49-51]; significantly, concentrations of both IL-12 and IL-2 were increased in tissue prepared from APP/PS1 mice, therefore, these infiltrating cells may be the source of the increase in IFNγ concentration in the brain of APP/PS1 mice providing the trigger for microglial activation and the consequent decrease in LTP. While an intact BBB provides one of the most important protective strategies for the brain limiting the entry of cells and preventing the entry of high molecular molecules, the evidence has indicated that its permeability is increased in AD [52, 53] and in mouse models of AD [54, 55], perhaps as a consequence of amyloidogenesis [56] since the age-related increase in fluorescence was magnified by the presence of Aβ plaque deposition in AD mice.

To assess whether IFNγ might provide the trigger for glial activation in this study, the effects of intracerebroventricular injection of IFNγ were evaluated and the data demonstrate that IFNγ increases activation of both microglia and astrocytes and is associated with increased expression of inflammatory cytokines. IFNγ also decreases LTP which concurs with earlier data indicating that IFNγ inhibited LTP in dentate gyrus of urethane-anaesthetized rats [57, 58] and with the observation that when hippocampal concentration of IFNγ is decreased, LTP is sustained [40]. Additionally, incubation of

primary isolated microglia with IFNγ showed similar effects in terms of proinflammatory cytokine release and the cell surface expression of the co-stimulatory molecule CD86 and MHCII which are important in microglial activation. Therefore these data suggest that IFNγ, probably derived from infiltrating cells has a detrimental effect, but it is important to note that a protective effect of infiltrating leukocytes has been reported [59], while infiltrating macrophages have been shown to limit Aβ accumulation [60].

It is not clear whether microglial activation precedes or follows Aβ deposition. Aβ certainly induces microglial activation *in vivo* and *in vitro* [1, 61] and it has been reported that MHCII immunoreactivity follows plaque formation in APP/PS1 mice [62] although CD11b immunoreactivity appears to coincide with plaque development in APP-overexpressing mice [63]. However, chronic inflammatory changes, presumably accompanied by glial activation, may precipitate Aβ deposition [64], whereas TNFα and IL-1β, which are released from activated microglia, increase activity and/or expression of γ- and β-secretases [4, 5] which ultimately leads to Aβ deposition. Careful longitudinal studies are necessary to establish the sequence of events and this may be facilitated by MRI analysis of T_1 and T_2 relaxation times.

The evidence supports the hypothesis that infiltration of peripheral cells, specifically macrophages and NK cells, is likely to contribute to the inflammatory microenvironment in the brain, perhaps by providing a source of IFNγ which triggers glial activation and release of inflammatory mediators that ultimately negatively impact on synaptic plasticity.

ACKNOWLEDGEMENTS

This work was funded by Science Foundation Ireland (07/IN.1/B949). RK was supported by a postgraduate studentship from the Dublin Region Higher Education Alliance funded by the Strategic Innovation Fund (Cycle 2; HEA 2008) from the Higher Education Authority. RSJ and TCB were supported by a Health Research Board-funded structured PhD program in Neuroscience (PhD/2008/13). The funders had no role in study design, data collection and analysis, decision to publish, or preparation of the manuscript.

REFERENCES

[1] Clarke RM, O'Connell F, Lyons A, Lynch MA (2007) The HMG-CoA reductase inhibitor, atorvastatin, attenuates the effects of acute administration of amyloid-beta1-42 in the rat hippocampus in vivo. *Neuropharmacology* **52**, 136-145.

[2] Lyons A, Griffin RJ, Costelloe CE, Clarke RM, Lynch MA (2007) IL-4 attenuates the neuroinflammation induced by amyloid-beta in vivo and in vitro. *J Neurochem* **101**, 771-781.

[3] Glass CK, Saijo K, Winner B, Marchetto MC, Gage FH (2010) Mechanisms underlying inflammation in neurodegeneration. *Cell* **140**, 918-934.

[4] Liao YF, Wang BJ, Cheng HT, Kuo LH, Wolfe MS (2004) Tumor necrosis factor-alpha, interleukin-1beta, and interferon-gamma stimulate gamma-secretase-mediated cleavage of amyloid precursor protein through a JNK-dependent MAPK pathway. *J Biol Chem* **279**, 49523-49532.

[5] Sastre M, Walter J, Gentleman SM (2008) Interactions between APP secretases and inflammatory mediators. *J Neuroinflammation* **5**, 25.

[6] Kitazawa M, Cheng D, Tsukamoto MR, Koike MA, Wes PD, Vasilevko V, Cribbs DH, LaFerla FM (2011) Blocking IL-1 signaling rescues cognition, attenuates tau pathology, and restores neuronal beta-catenin pathway function in an Alzheimer's disease model. *J Immunol* **187**, 6539-6549.

[7] Giunta B, Fernandez F, Nikolic WV, Obregon D, Rrapo E, Town T, Tan J (2008) Inflammaging as a prodrome to Alzheimer's disease. *J Neuroinflammation* **5**, 51.

[8] Choi SH, Aid S, Kim HW, Jackson SH, Bosetti F (2012) Inhibition of NADPH oxidase promotes alternative and anti-inflammatory microglial activation during neuroinflammation. *J Neurochem* **120**, 292-301.

[9] Reed-Geaghan EG, Reed QW, Cramer PE, Landreth GE (2010) Deletion of CD14 attenuates Alzheimer's disease pathology by influencing the brain's inflammatory milieu. *J Neurosci* **30**, 15369-15373.

[10] van Walderveen MA, Kamphorst W, Scheltens P, van Waesberghe JH, Ravid R, Valk J, Polman CH, Barkhof F (1998) Histopathologic correlate of hypointense lesions on T1-weighted spin-echo MRI in multiple sclerosis. *Neurology* **50**, 1282-1288.

[11] Barnes D, McDonald WI, Landon DN, Johnson G (1988) The characterization of experimental gliosis by quantitative nuclear magnetic resonance imaging. *Brain* **111 (Pt 1)**, 83-94.

[12] Gallagher JJ, Finnegan ME, Grehan B, Dobson J, Collingwood JF, Lynch MA (2012) Modest amyloid deposition is associated with iron dysregulation, microglial activation, and oxidative stress. *J Alzheimers Dis* **28**, 147-161.

[13] Helpern JA, Lee SP, Falangola MF, Dyakin VV, Bogart A, Ardekani B, Duff K, Branch C, Wisniewski T, de Leon MJ, Wolf O, O'Shea J, Nixon RA (2004) MRI assessment of neuropathology in a transgenic mouse model of Alzheimer's disease. *Magn Reson Med* **51**, 794-798.

[14] Bartzokis G, Sultzer D, Cummings J, Holt LE, Hance DB, Henderson VW, Mintz J (2000) In vivo evaluation of brain iron in Alzheimer disease using magnetic resonance imaging. *Arch Gen Psychiatry* **57**, 47-53.

[15] Sibson NR, Lowe JP, Blamire AM, Martin MJ, Obrenovitch TP, Anthony DC (2008) Acute astrocyte activation in brain detected by MRI: new insights into T(1) hypointensity. *J Cereb Blood Flow Metab* **28**, 621-632.

[16] Justicia C, Ramos-Cabrer P, Hoehn M (2008) MRI detection of secondary damage after stroke: chronic iron accumulation in the thalamus of the rat brain. *Stroke* **39**, 1541-1547.

[17] Costello DA, Watson MB, Cowley TR, Murphy N, Murphy Royal C, Garlanda C, Lynch MA (2011) Interleukin-1alpha and HMGB1 mediate hippocampal dysfunction in SIGIRR-deficient mice. *J Neurosci* **31**, 3871-3879.

[18] Blau CW, Cowley TR, O'Sullivan J, Grehan B, Browne TC, Kelly L, Birch A, Murphy N, Kelly AM, Kerskens CM, Lynch MA (2011) The age-related deficit in LTP is associated with changes in perfusion and blood-brain barrier permeability. *Neurobiol Aging*.

[19] Tuominen VJ, Ruotoistenmaki S, Viitanen A, Jumppanen M, Isola J (2010) ImmunoRatio: a publicly available web application for quantitative image analysis of estrogen receptor (ER), progesterone receptor (PR), and Ki-67. *Breast Cancer Res* **12**, R56.

[20] Cowley TR, O'Sullivan J, Blau C, Deighan BF, Jones R, Kerskens C, Richardson JC, Virley D, Upton N, Lynch MA (2012) Rosiglitazone attenuates the age-related changes in astrocytosis and the deficit in LTP. *Neurobiol Aging* **33**, 162-175.

[21] Tancredi V, Zona C, Velotti F, Eusebi F, Santoni A (1990) Interleukin-2 suppresses established long-term potentiation and inhibits its induction in the rat hippocampus. *Brain Res* **525**, 149-151.

[22] Costelloe C, Watson M, Murphy A, McQuillan K, Loscher C, Armstrong ME, Garlanda C, Mantovani A, O'Neill LA, Mills KH, Lynch MA (2008) IL-1F5 mediates anti-inflammatory activity in the brain through induction of IL-4 following interaction with SIGIRR/TIR8. *J Neurochem* **105**, 1960-1969.

[23] Aso E, Lomoio S, Lopez-Gonzalez I, Joda L, Carmona M, Fernandez-Yague N, Moreno J, Juves S, Pujol A, Pamplona R, Portero-Otin M, Martin V, Diaz M, Ferrer I (2011) Amyloid Generation and Dysfunctional Immunoproteasome Activation with Disease Progression in Animal Model of Familial Alzheimer's Disease. *Brain Pathol*.

[24] Jankowsky JL, Fadale DJ, Anderson J, Xu GM, Gonzales V, Jenkins NA, Copeland NG, Lee MK, Younkin LH, Wagner SL, Younkin SG, Borchelt DR (2004) Mutant presenilins specifically elevate the levels of the 42 residue beta-amyloid peptide in vivo: evidence for augmentation of a 42-specific gamma secretase. *Hum Mol Genet* **13**, 159-170.

[25] Scott L, Feng J, Kiss T, Needle E, Atchison K, Kawabe TT, Milici AJ, Hajos-Korcsok E, Riddell D, Hajos M (2012) Age-dependent disruption in hippocampal theta oscillation in amyloid-beta overproducing transgenic mice. *Neurobiol Aging*.

[26] Garcia-Alloza M, Robbins EM, Zhang-Nunes SX, Purcell SM, Betensky RA, Raju S, Prada C, Greenberg SM, Bacskai BJ, Frosch MP (2006) Characterization of amyloid deposition in the APPswe/PS1dE9 mouse model of Alzheimer disease. *Neurobiol Dis* **24**, 516-524.

[27] O'Reilly JA, Lynch M (2012) Rosiglitazone improves spatial memory and decreases insoluble Abeta(1-42) in APP/PS1 mice. *J Neuroimmune Pharmacol* **7**, 140-144.

[28] Sanchez-Ramos J, Song S, Sava V, Catlow B, Lin X, Mori T, Cao C, Arendash GW (2009) Granulocyte colony stimulating factor decreases brain amyloid burden and reverses cognitive impairment in Alzheimer's mice. *Neuroscience* **163**, 55-72.

[29] Venneti S, Lopresti BJ, Wang G, Hamilton RL, Mathis CA, Klunk WE, Apte UM, Wiley CA (2009) PK11195 labels activated microglia in Alzheimer's disease and in vivo in a mouse model using PET. *Neurobiol Aging* **30**, 1217-1226.

[30] Teipel SJ, Kaza E, Hadlich S, Bauer A, Bruning T, Plath AS, Krohn M, Scheffler K, Walker LC, Lotze M, Pahnke J (2011) Automated Detection of Amyloid-beta-Related Cortical and Subcortical Signal Changes ina Transgenic Model of Alzheimer's Disease using High-Field MRI. *J Alzheimers Dis* **23**, 221-237.

[31] Falangola MF, Lee SP, Nixon RA, Duff K, Helpern JA (2005) Histological co-localization of iron in Abeta plaques of PS/APP transgenic mice. *Neurochem Res* **30**, 201-205.

[32] El Tannir El Tayara N, Delatour B, Le Cudennec C, Guegan M, Volk A, Dhenain M (2006) Age-related evolution of amyloid burden, iron load, and MR relaxation times in a transgenic mouse model of Alzheimer's disease. *Neurobiol Dis* **22**, 199-208.

[33] Mei X, Ezan P, Giaume C, Koulakoff A (2010) Astroglial connexin immunoreactivity is specifically altered at beta-amyloid plaques in beta-amyloid precursor protein/presenilin1 mice. *Neuroscience* **171**, 92-105.

[34] Puolivali J, Bjorklund M, Holmberg M, Ihalainen JA, Scheinin M, Tanila H (2002) Alpha 2C-adrenoceptor mediated regulation of cortical EEG arousal. *Neuropharmacology* **43**, 1305-1312.

[35] Liu L, Ikonen S, Heikkinen T, Tapiola T, van Groen T, Tanila H (2002) The effects of long-term treatment with metrifonate, a cholinesterase inhibitor, on cholinergic activity, amyloid pathology, and cognitive function in APP and PS1 doubly transgenic mice. *Exp Neurol* **173**, 196-204.

[36] Rosi S, Vazdarjanova A, Ramirez-Amaya V, Worley PF, Barnes CA, Wenk GL (2006) Memantine protects against LPS-induced neuroinflammation, restores behaviorally-induced gene expression and spatial learning in the rat. *Neuroscience* **142**, 1303-1315.

[37] Iwasaki K, Egashira N, Takagaki Y, Yoshimitsu Y, Hatip-Al-Khatib I, Mishima K, Fujiwara M (2007) Nilvadipine prevents the impairment of spatial memory induced by cerebral ischemia combined with beta-amyloid in rats. *Biol Pharm Bull* **30**, 698-701.

[38] Prediger RD, Franco JL, Pandolfo P, Medeiros R, Duarte FS, Di Giunta G, Figueiredo CP, Farina M, Calixto JB, Takahashi RN, Dafre AL (2007) Differential susceptibility following beta-amyloid peptide-(1-40) administration in C57BL/6 and Swiss albino mice: Evidence for a dissociation between cognitive deficits and the glutathione system response. *Behav Brain Res* **177**, 205-213.

[39] Ma T, Klann E (2012) Amyloid beta: linking synaptic plasticity failure to memory disruption in Alzheimer's disease. *J Neurochem* **120 Suppl 1**, 140-148.

[40] Clarke RM, Lyons A, O'Connell F, Deighan BF, Barry CE, Anyakoha NG, Nicolaou A, Lynch MA (2008) A pivotal role for interleukin-4 in atorvastatin-associated neuroprotection in rat brain. *J Biol Chem* **283**, 1808-1817.

[41] Loane DJ, Deighan BF, Clarke RM, Griffin RJ, Lynch AM, Lynch MA (2009) Interleukin-4 mediates the neuroprotective effects of rosiglitazone in the aged brain. *Neurobiol Aging* **30**, 920-931.

[42] Gruart A, Lopez-Ramos JC, Munoz MD, Delgado-Garcia JM (2008) Aged wild-type and APP, PS1, and APP + PS1 mice present similar deficits in associative learning and synaptic plasticity independent of amyloid load. *Neurobiol Dis* **30**, 439-450.

[43] Gureviciene I, Ikonen S, Gurevicius K, Sarkaki A, van Groen T, Pussinen R, Ylinen A, Tanila H (2004) Normal induction but accelerated decay of LTP in APP + PS1 transgenic mice. *Neurobiol Dis* **15**, 188-195.

[44] Tan J, Town T, Paris D, Mori T, Suo Z, Crawford F, Mattson MP, Flavell RA, Mullan M (1999) Microglial activation resulting from CD40-CD40L interaction after beta-amyloid stimulation. *Science* **286**, 2352-2355.

[45] Lebbadi M, Julien C, Phivilay A, Tremblay C, Emond V, Kang JX, Calon F (2011) Endogenous conversion of omega-6 into omega-3 fatty acids improves neuropathology in an animal model of Alzheimer's disease. *J Alzheimers Dis* **27**, 853-869.

[46] Kelly L, Grehan B, Chiesa AD, O'Mara SM, Downer E, Sahyoun G, Massey KA, Nicolaou A, Lynch MA (2011) The polyunsaturated fatty acids, EPA and DPA exert a protective effect in the hippocampus of the aged rat. *Neurobiol Aging* **32**, 2318 e2311-2315.

[47] Downer EJ, Cowley TR, Cox F, Maher FO, Berezin V, Bock E, Lynch MA (2009) A synthetic NCAM-derived mimetic peptide, FGL, exerts anti-inflammatory properties via IGF-1 and interferon-gamma modulation. *J Neurochem* **109**, 1516-1525.

[48] Benveniste EN, Nguyen VT, Wesemann DR (2004) Molecular regulation of CD40 gene expression in macrophages and microglia. *Brain Behav Immun* **18**, 7-12.

[49] Lyons A, Murphy KJ, Clarke R, Lynch MA (2011) Atorvastatin prevents age-related and amyloid-beta-induced microglial activation by blocking interferon-gamma release from natural killer cells in the brain. *J Neuroinflammation* **8**, 27.

[50] Pintaric M, Gerner W, Saalmuller A (2008) Synergistic effects of IL-2, IL-12 and IL-18 on cytolytic activity, perforin expression and IFN-gamma production of porcine natural killer cells. *Vet Immunol Immunopathol* **121**, 68-82.

[51] Schindler H, Lutz MB, Rollinghoff M, Bogdan C (2001) The production of IFN-gamma by IL-12/IL-18-activated macrophages requires STAT4 signaling and is inhibited by IL-4. *J Immunol* **166**, 3075-3082.

[52] Starr JM, Farrall AJ, Armitage P, McGurn B, Wardlaw J (2009) Blood-brain barrier permeability in Alzheimer's disease: a case-control MRI study. *Psychiatry Res* **171**, 232-241.

[53] Farrall AJ, Wardlaw JM (2009) Blood-brain barrier: ageing and microvascular disease--systematic review and meta-analysis. *Neurobiol Aging* **30**, 337-352.

[54] Ujiie M, Dickstein DL, Carlow DA, Jefferies WA (2003) Blood-brain barrier permeability precedes senile plaque formation in an Alzheimer disease model. *Microcirculation* **10**, 463-470.

[55] Paul J, Strickland S, Melchor JP (2007) Fibrin deposition accelerates neurovascular damage and neuroinflammation in mouse models of Alzheimer's disease. *J Exp Med* **204**, 1999-2008.

[56] Biron KE, Dickstein DL, Gopaul R, Jefferies WA (2011) Amyloid triggers extensive cerebral angiogenesis causing blood brain barrier permeability and hypervascularity in Alzheimer's disease. *PLoS One* **6**, e23789.

[57] Maher FO, Clarke RM, Kelly A, Nally RE, Lynch MA (2006) Interaction between interferon gamma and insulin-like growth factor-1 in hippocampus impacts on the ability of rats to sustain long-term potentiation. *J Neurochem* **96**, 1560-1571.

[58] Lynch AM, Loane DJ, Minogue AM, Clarke RM, Kilroy D, Nally RE, Roche OJ, O'Connell F, Lynch MA (2007) Eicosapentaenoic acid confers neuroprotection in the amyloid-beta challenged aged hippocampus. *Neurobiol Aging* **28**, 845-855.

[59] Yong VW, Rivest S (2009) Taking advantage of the systemic immune system to cure brain diseases. *Neuron* **64**, 55-60.

[60] Town T, Laouar Y, Pittenger C, Mori T, Szekely CA, Tan J, Duman RS, Flavell RA (2008) Blocking TGF-beta-Smad2/3 innate immune signaling mitigates Alzheimer-like pathology. *Nat Med* **14**, 681-687.

[61] Lyons A, Downer EJ, Crotty S, Nolan YM, Mills KH, Lynch MA (2007) CD200 ligand receptor interaction modulates microglial activation in vivo and in vitro: a role for IL-4. *J Neurosci* **27**, 8309-8313.

[62] Gordon MN, Holcomb LA, Jantzen PT, DiCarlo G, Wilcock D, Boyett KW, Connor K, Melachrino J, O'Callaghan JP, Morgan D (2002) Time course of the development of Alzheimer-like pathology in the doubly transgenic PS1+APP mouse. *Exp Neurol* **173**, 183-195.

[63] Dudal S, Krzywkowski P, Paquette J, Morissette C, Lacombe D, Tremblay P, Gervais F (2004) Inflammation occurs early during the Abeta deposition process in TgCRND8 mice. *Neurobiol Aging* **25**, 861-871.

[64] Morgan D, Gordon MN, Tan J, Wilcock D, Rojiani AM (2005) Dynamic complexity of the microglial activation response in transgenic models of amyloid deposition: implications for Alzheimer therapeutics. *J Neuropathol Exp Neurol* **64**, 743-753.

FIGURE LEGENDS

Figure 1: Microglial activation is increased in APP/PS1 mice

A-D. T_2 relaxation time was decreased (as indicated by a change from red/yellow to blue colours) in several areas of the brain of APP/PS1 (B), compared with wildtype (A), mice. (An indicator of time (msec) and colour is presented). C,D. A significant decrease in T_2 relaxation time was observed in the cortex (C) and hippocampus (D) of APP/PS1, compared with wildtype, mice (*$p < 0.05$; ***$p < 0.001$; Student's *t*-test for Independent means). CD11b immunoreactivity was markedly greater in cortex (F) and hippocampus (H) of APP/PS1 mice compared with wildtype mice (E and G respectively) and quantitative analysis of the DAB-enhanced images revealed a significant increase in cortex (I) and hippocampus (J; ***$p < 0.001$; Student's *t*-test for Independent means). K. CD11b mRNA was significantly increased in tissue prepared from APP/PS1 mice (***$p < 0.001$; Student's *t*-test for Independent means; n=7 for wildtype mice and n=9 for APP/PS1 mice). L,M. The number of $CD11b^+$ cells which also stained positively for CD68 was significantly increased in tissue prepared from APP/PS1 mice (***$p < 0.001$; Student's *t*-test for Independent means).

Figure 2: GFAP immunoreactivity and GFAP mRNA expression are increased in tissue prepared from APP/PS1 mice

A-D. T_1 relaxation time was increased (as indicated by a change from green/yellow to orange/red colours) in several areas of the brain of APP/PS1, compared with wildtype , mice (compare B with A). (An indicator of time (msec) and colour is presented). C,D. A significant increase in T_1 relaxation time was observed in the cortex (C) and hippocampus

(D) of APP/PS1, compared with wildtype, mice (*p < 0.05; **p < 0.01; Student's *t*-test for Independent means). E-H. GFAP immunoreactivity was markedly increased in sections prepared from the cortex of APP/PS1 (F), compared with wildtype (E) mice and in hippocampus of APP/PS1 (H), compared with wildtype (G) mice and quantitative analysis of the DAB-enhanced images revealed a significant increase in cortex (I) and hippocampus (J; ***p < 0.001; Student's *t*-test for Independent means). K. GFAP mRNA was significantly increased in tissue prepared from APP/PS1 mice compared with wildtype mice (***p < 0.001; Student's *t*-test for Independent means).

Figure 3: Increased concentrations of inflammatory cytokines in hippocampus of APP/PS1 are associated with a deficit in LTP.

Hippocampal concentrations of IL-1β (A), TNFα (B), IL-2 (C) and IL-12 (D) were significantly greater in tissue prepared from APP/PS1, compared with wildtype, mice (*p < 0.05; **p < 0.01; ***p < 0.001; Student's *t*-test for Independent means). (E) TBS-induced LTP, measured 60 min following induction, was significantly impaired in slices prepared from APP/PS1 mice (n = 3 slices from 3 animals) compared with that recorded from wildtype littermate controls (n = 4 slices from 3 animals; p < 0.0001, Student's *t*-test for Independent means). Data are presented as mean % EPSP slope ± SEM, the arrow represents application of TBS and the inset illustrates representative EPSP traces (averaged from 4 consecutive recordings), taken immediately prior to, and 60 min following, LTP induction (scale: 1mV / 20ms).

Figure 4: Macrophage and NK cell numbers are increased in the brain of APP/PS1 mice.

A. Hippocampal concentration of IFNγ was significantly greater in tissue prepared from APP/PS1, compared with wildtype, mice (**p < 0.01; Student's *t*-test for Independent means). B. The number of NK cells was also significantly increased in tissue prepared from APP/PS1, compared with wildtype, mice (***p < 0.001; Student's *t*-test for Independent means). C,D There was a significant increase in the percentage of $CD11b^{+}CD45^{hi}$ cells (macrophages) in the brain of APP/PS1 mice compared with their wildtype controls (C; ***p < 0.001; Student's *t*-test for Independent means) and expression of CD68 on these cells was significantly increased in brain tissue prepared from APP/PS1, compared with wildtype, mice (D; **p < 0.01; Student's *t*-test for Independent means).

Figure 5: IFNγ induces microglial activation and decreases LTP.

IFNγ (icv; 5µl; 50ng/ml) induced an increase in CD11b immunoreactivity (A) and GFAP immunoreactivity (C) in hippocampal sections (scale bar = 100µm). Expression of MHCII (B), GFAP (D), TNFα (E) and IL-6 (F) mRNA was increased in hippocampal tissue prepared from IFNγ-treated, compared with control-treated, mice (*p < 0.05; **p < 0.01; Student's *t*-test for Independent means). (G) Application of IFNγ (1µg/ml) to hippocampal slices, for 30 min prior to TBS-induced LTP, significantly impaired mean % EPSP slope (n = 5 slices) compared with that recorded under control conditions (n = 5 slices; p < 0.01, Student's *t*-test for Independent means), for 60 min following induction. Data are presented as mean % EPSP slope ± SEM. Arrow represents application of TBS. The inset illustrates representative EPSP

traces (averaged from 4 consecutive recordings), taken immediately prior to, and 60 min following LTP induction (scale: 1mV / 20ms).

Figure 6: IFNγ induces an increase in cell surface molecule expression and cytokine release *in vitro*

IFNγ (50ng/ml) induced an increase in the expression of CD86 (A) and MHCII (B) on the surface of isolated primary microglia (***p<0.001; Student's *t*-test for Independent means). The release of proinflammatory cytokines TNFα and IL-6 was significantly enhanced from microglia that had been treated with IFNγ in comparison to vehicle-treated controls (***p<0.001; Student's *t*-test for Independent means).

Supplementary Figure 1: T_2 relaxation time is decreased and CD11b expression is increased in aged wiltype mice.

A significant decrease in T_2 relaxation time was observed with increasing age in the hippocampus of wildtype mice (A; An indicator of colour is presented). CD11b immunoreactivity was markedly greater in hippocampus of aged wildtype mice, compared with their younger counterparts (B).

Table 1

	Wildtype	**APP/PS1**
Soluble $A\beta_{1-40}$ (pg/mg)	24.68 (5.08)	4052 (587.4)***
Insoluble $A\beta_{1-40}$ (pg/mg)	1.38 (0.67)	1779 (537.1)*
Soluble $A\beta_{1-42}$ (pg/mg)	15.43 (5.61)	2030 (274.4)***

Insoluble $A\beta_{1-42}$ (pg/mg)	0.14 (0.14)	2497 (555.3)**
Serum $A\beta_{1-40}$ (pg/ml)	17.20 (2.3)	142.5 (53.0)
Serum $A\beta_{1-42}$ (pg/ml)	0.76 (0.46)	14.96 (6.22)

Aβ deposition is increased in tissue prepared from APP/PS1 mice.

Concentrations of soluble and insoluble $A\beta_{1-40}$ and $A\beta_{1-42}$ were significantly increased in tissue prepared from APP/PS1, compared with wildtype, mice (*$p < 0.05$; **$p < 0.01$; ***$p < 0.001$; Student's *t*-test for Independent means; n=7 for wildtype mice and n=9 for APP/PS1 mice). The increases in serum concentrations of $A\beta_{1-40}$ and $A\beta_{1-42}$ in APP/PS1 mice did not reach statistical significance.

Table 2

		Wildtype	**APP/PS1**	**Significance**
Whole Cortex	**T_1**	1685	1663	NS
	T_2	49.44	48.49	*
Motor Cortex	**T_1**	1579	1682	**
	T_2	49.64	46.36	***
Entorhinal Cortex	**T_1**	1689	1692	NS
	T_2	50.77	48.79	***
Hippocampus	**T_1**	1631	1688	*
	T_2	49.98	48.72	*
Corpus Callosum	**T_1**	1535	1509	NS
	T_2	43.46	42.61	NS

Thalamus	**T_1**	1369	1418	NS
	T_2	42.95	43.07	NS

Mean values for T_1 and T_2 relaxation times (msec) in different brain areas are given for wildtype and APP/PS1 mice. Significant genotype-related increases in T_1 relaxation times were observed in the motor cortex and hippocampus, whereas significant decreases in T_2 relaxation times were observed in the whole cortex, motor cortex, entorhinal cortex and hippocampus (*$p < 0.05$; **$p < 0.01$; ***$p < 0.001$; Student's *t*-test for Independent means). No significant changes in either T_1 or T_2 relaxation times were observed in the corpus callosum or thalamus.

Figure 1

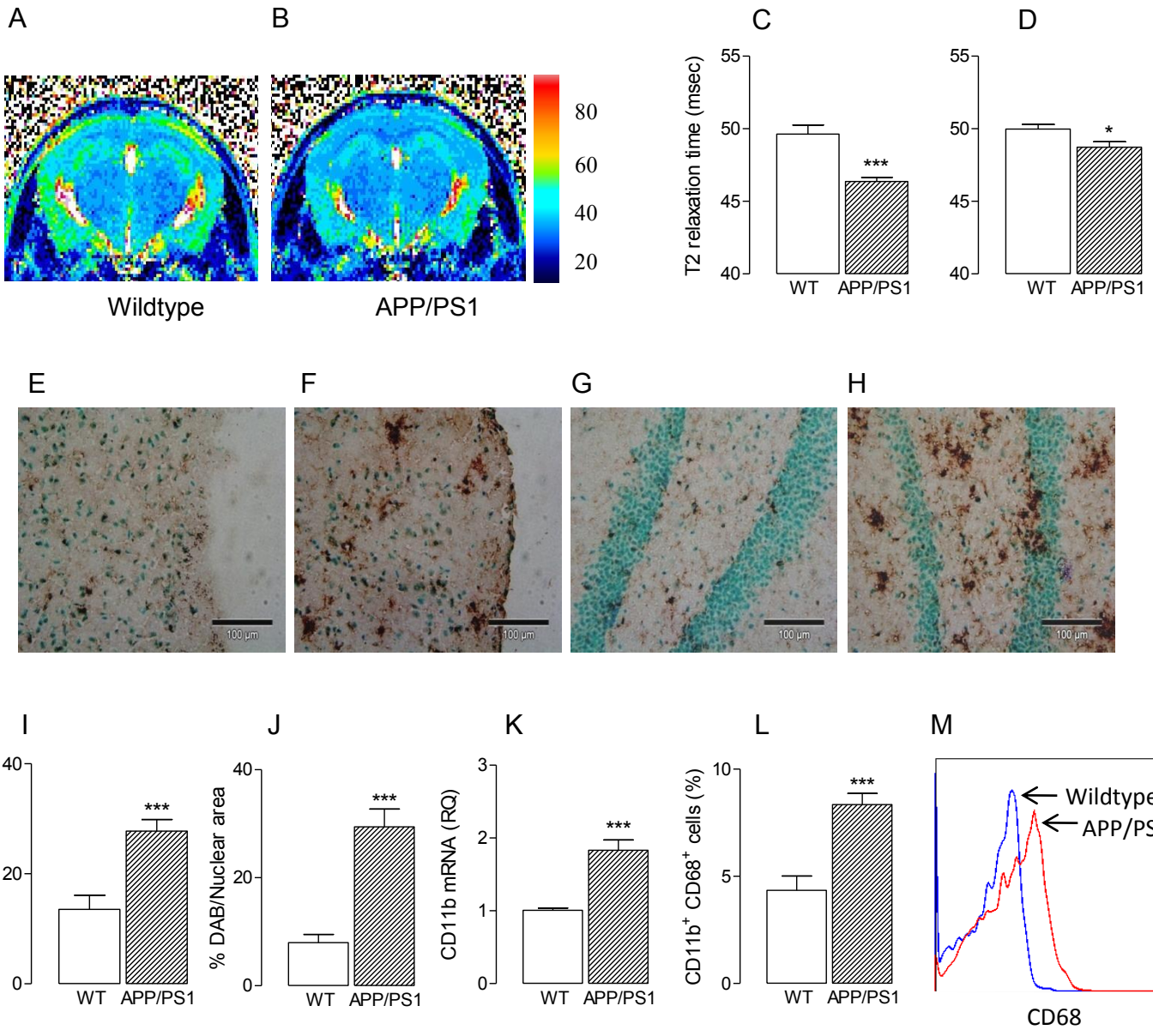
A
B
C
D
80
60
40
20
Wildtype
APP/PS1
T2 relaxation time (msec)
55
50
45
40
***
*
WT
APP/PS1
E
F
G
H
100 µm
I
J
K
L
M
% DAB/Nuclear area
40
20
0
***
WT
APP/PS1
CD11b mRNA (RQ)
3
2
1
CD11b+ CD68+ cells (%)
10
5
Wildtype
APP/PS1
CD68

Figure 2

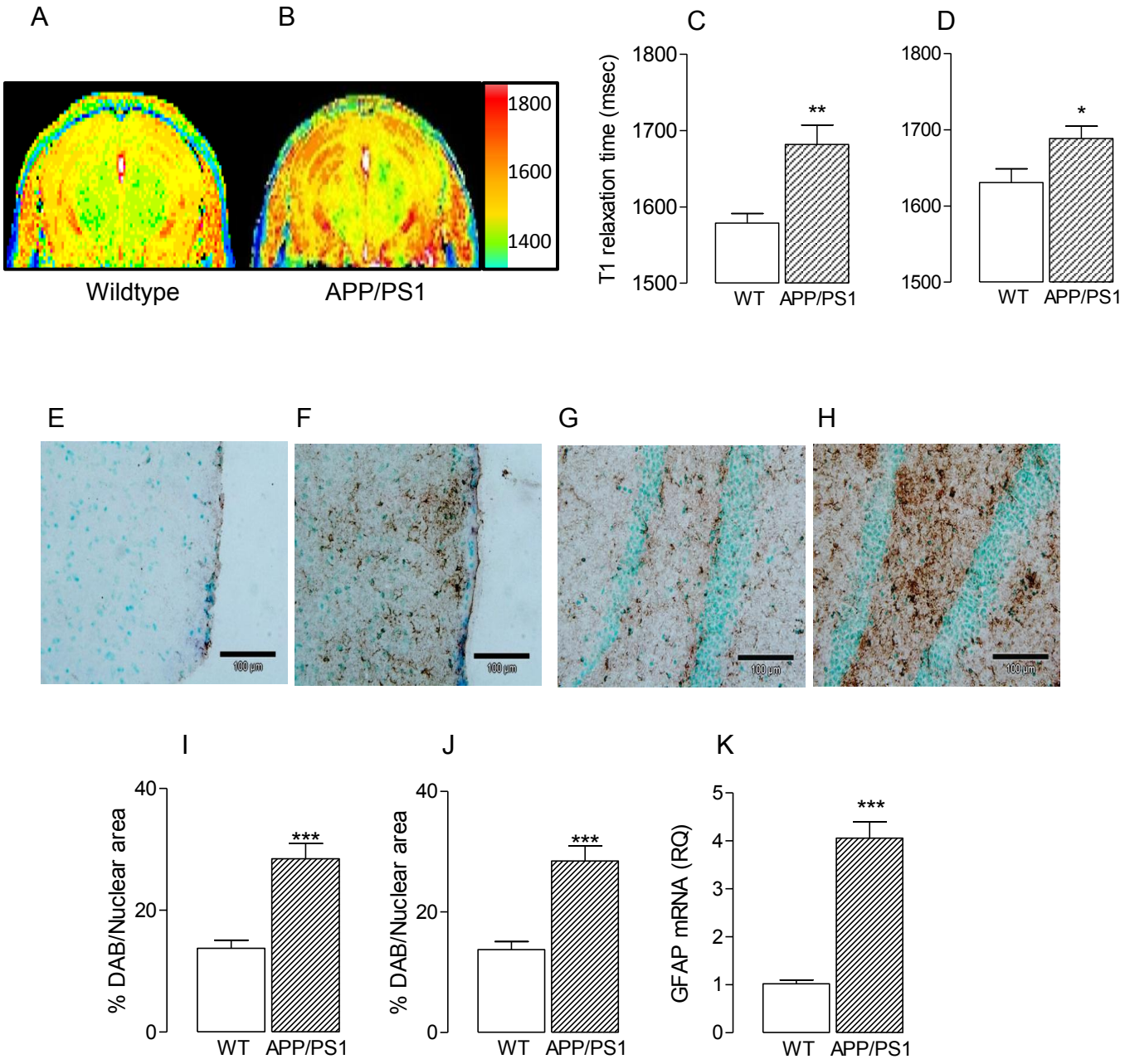
A
B
C
D
1800
1600
1400
Wildtype
APP/PS1
T1 relaxation time (msec)
1800
1700
1600
1500
**
WT
APP/PS1
1800
1700
1600
1500
*
WT
APP/PS1
E
F
G
H
100 µm
100 µm
100 µm
100 µm
I
J
K
% DAB/Nuclear area
40
20
0
***
WT
APP/PS1
% DAB/Nuclear area
40
20
0
***
WT
APP/PS1
GFAP mRNA (RQ)
5
4
3
2
1
0
***
WT
APP/PS1

Figure 3

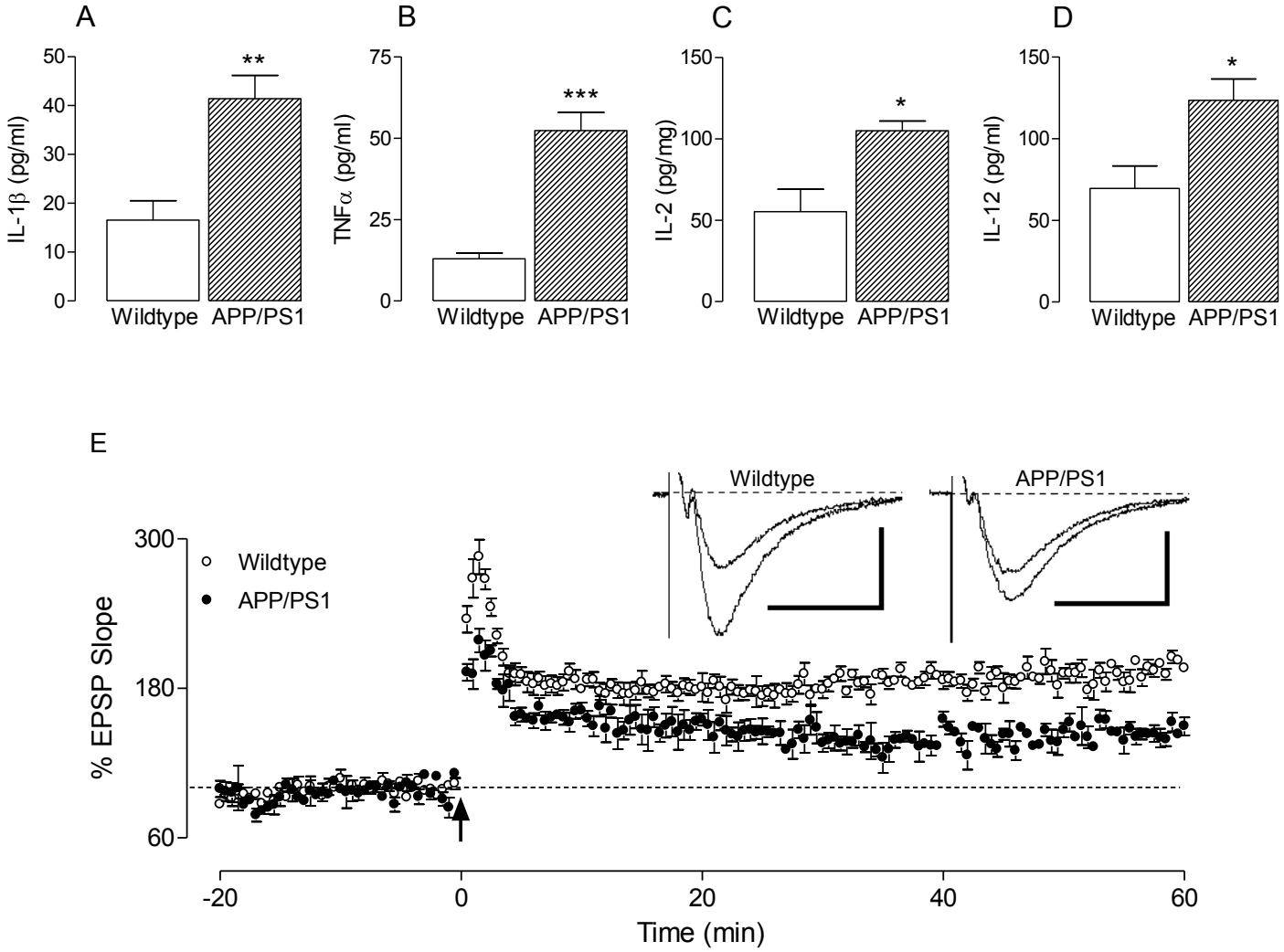
A
B
C
D
IL-1β (pg/ml)
TNFα (pg/ml)
IL-2 (pg/mg)
IL-12 (pg/ml)
Wildtype
APP/PS1
**
***
*
*
E
Wildtype
APP/PS1
% EPSP Slope
Time (min)

Figure 4

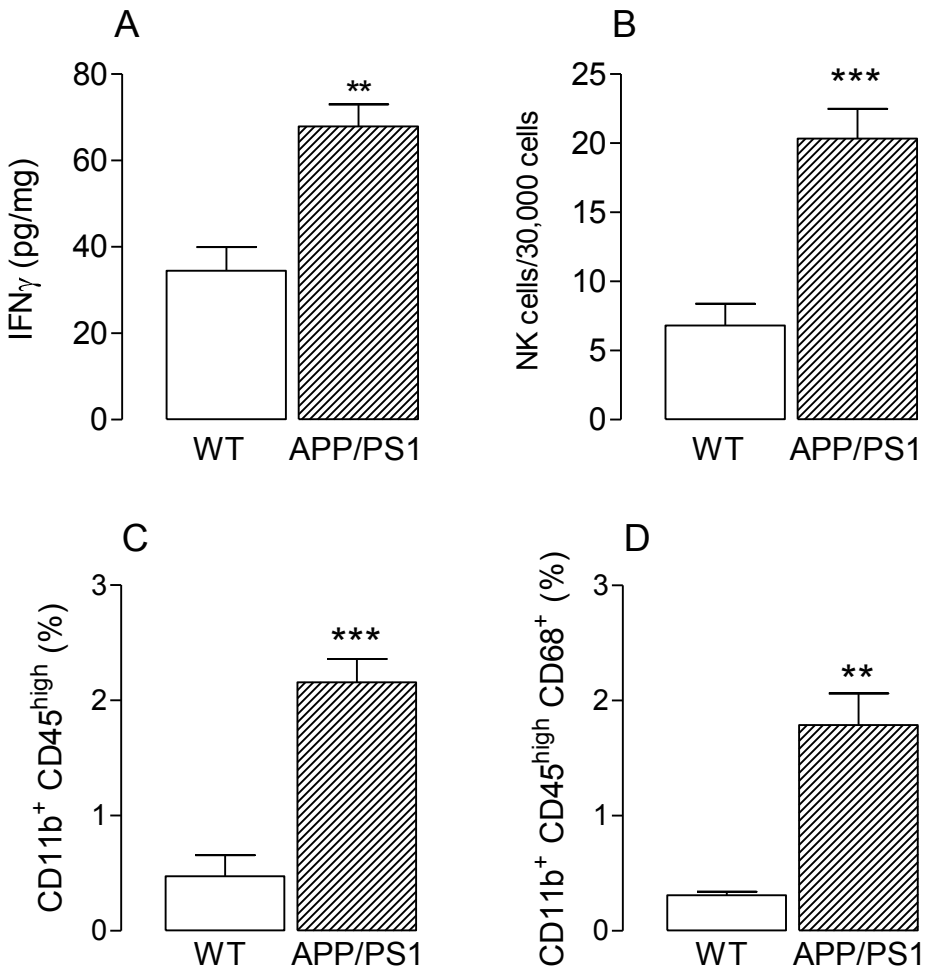
A
IFNγ (pg/mg)
80
60
40
20
0
**
WT
APP/PS1
B
NK cells/30,000 cells
25
20
15
10
5
0
***
WT
APP/PS1
C
CD11b+ CD45high (%)
3
2
1
0
***
WT
APP/PS1
D
CD11b+ CD45high CD68+ (%)
3
2
1
0
**
WT
APP/PS1

Figure 5

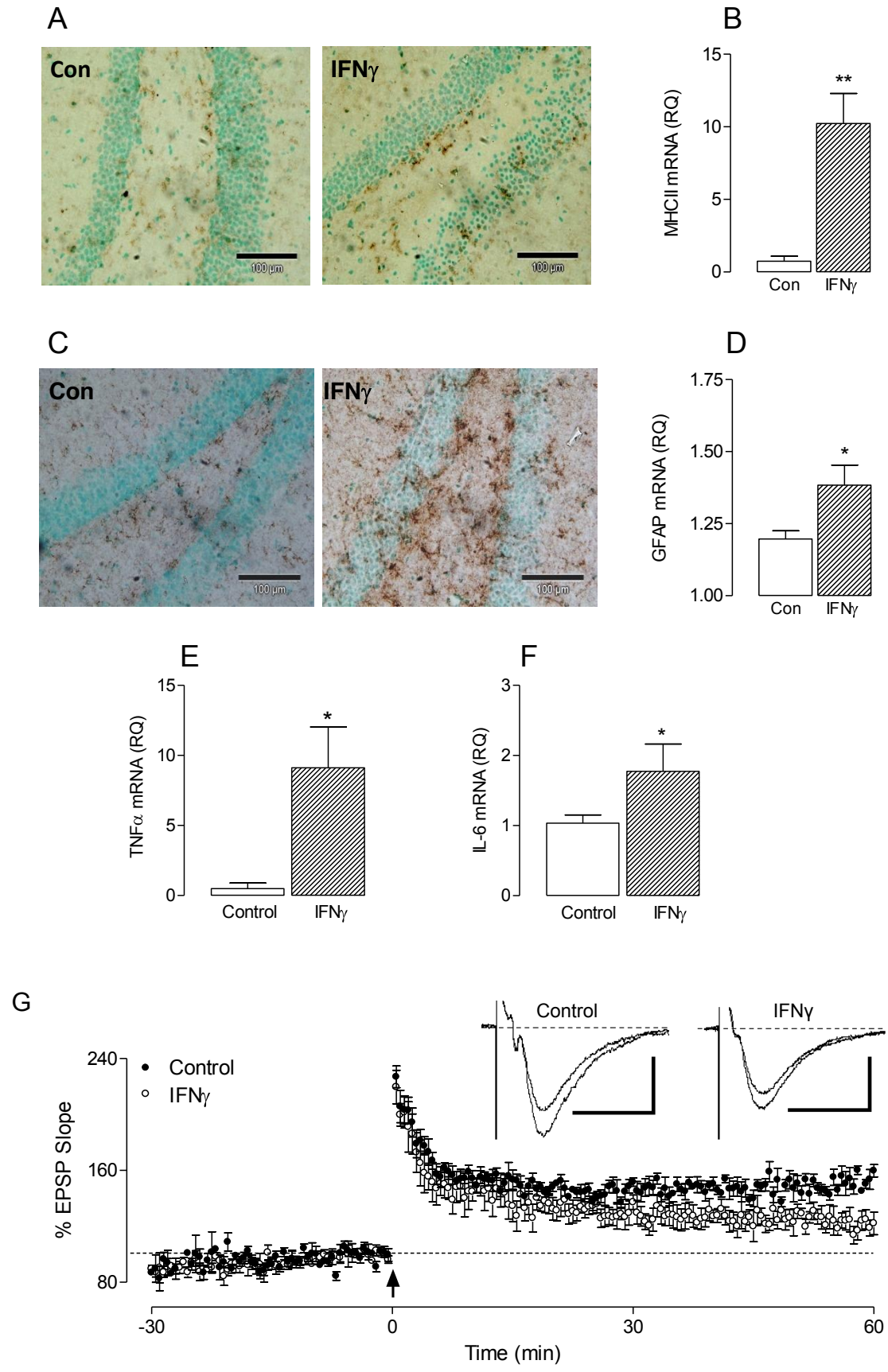
A
Con
IFNγ
100 µm
B
MHCII mRNA (RQ)
15
10
5
0
**
Con
IFNγ
C
Con
IFNγ
100 µm
D
GFAP mRNA (RQ)
1.75
1.50
1.25
1.00
*
Con
IFNγ
E
TNFα mRNA (RQ)
15
10
5
0
*
Control
IFNγ
F
IL-6 mRNA (RQ)
3
2
1
0
*
Control
IFNγ
G
Control
IFNγ
% EPSP Slope
240
160
80
Control
IFNγ
-30
0
30
60
Time (min)

Figure 6

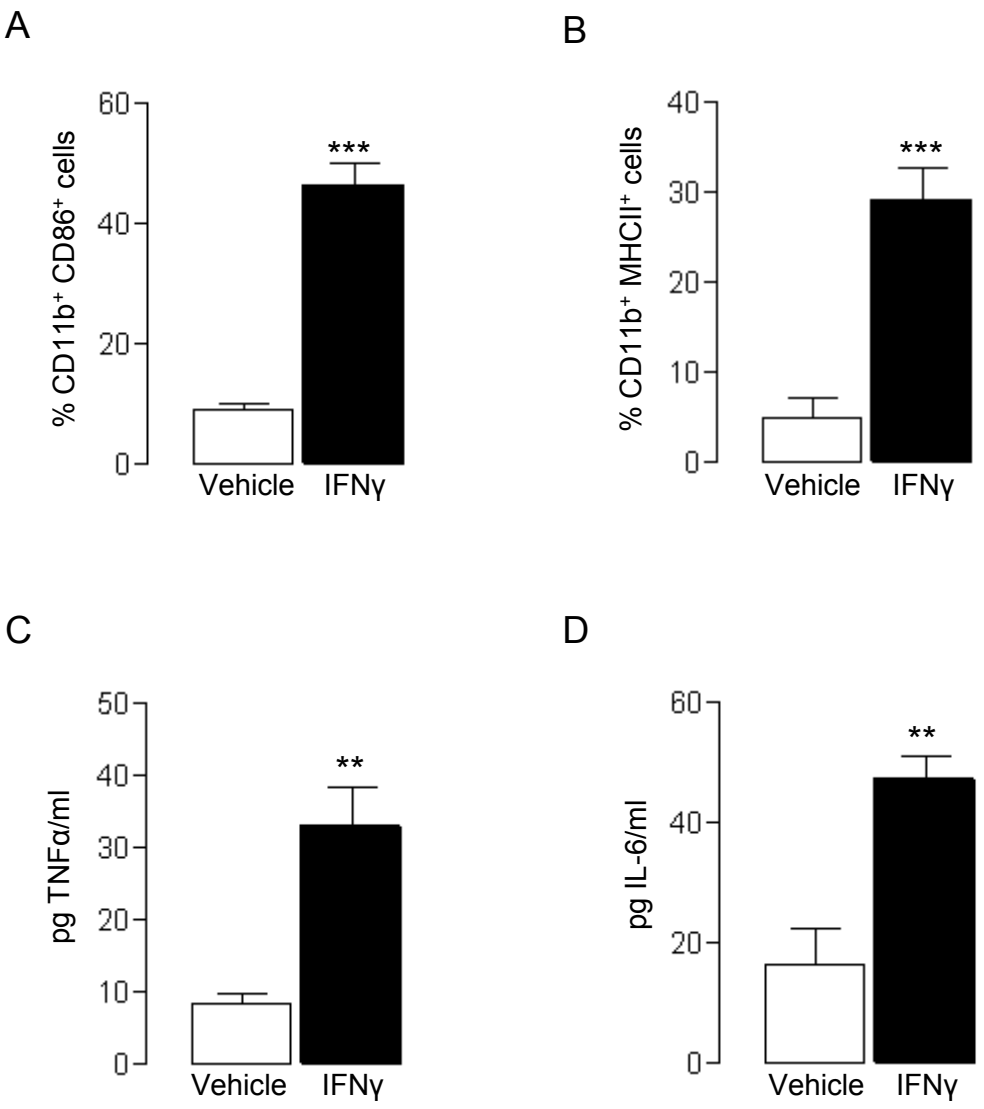
A
% CD11b+ CD86+ cells
60
40
20
0
***
Vehicle
IFNγ
B
% CD11b+ MHCII+ cells
40
30
20
10
0
***
Vehicle
IFNγ
C
pg TNFα/ml
50
40
30
20
10
0
**
Vehicle
IFNγ
D
pg IL-6/ml
60
40
20
0
**
Vehicle
IFNγ

Supplementary Figure 1

A

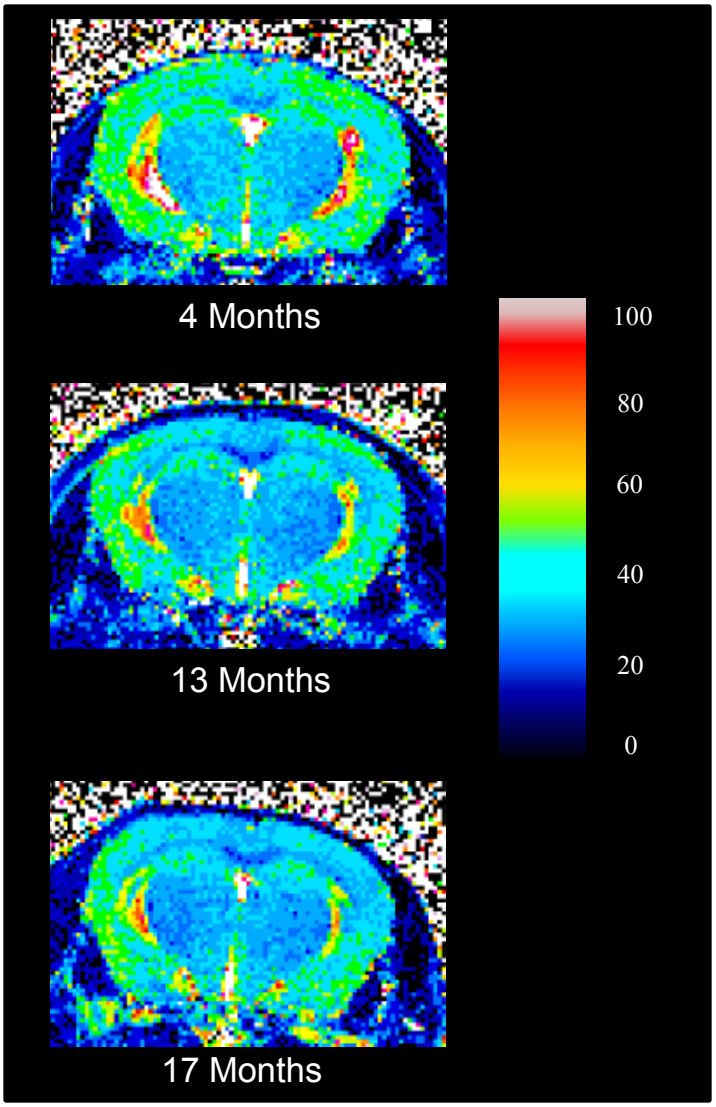

B

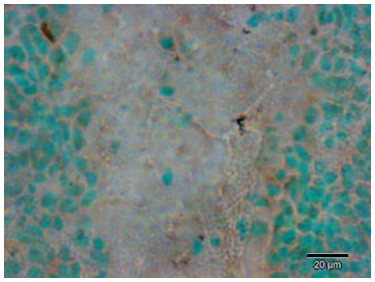

4 Months

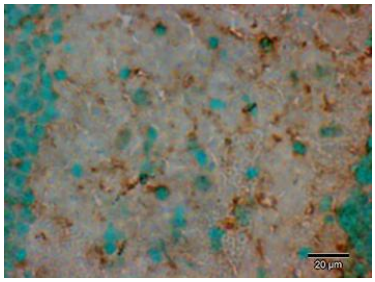

13 Months

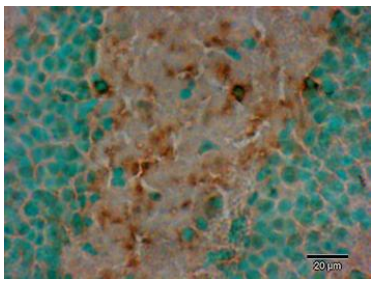

17 Months